A&A 655, A74 (2021)
https://doi.org/10.1051/0004-6361/202141190

Astronomy & Astrophysics

Sulfur ion irradiation experiments simulating space weathering of Solar System body surfaces

Organosulfur compound formation*

Alexander Ruf[1,2], Alexis Bouquet[1], Philippe Schmitt-Kopplin[3,4], Philippe Boduch[5], Olivier Mousis[6], and Grégoire Danger[1,6,7]

[1] Université Aix-Marseille, CNRS, Laboratoire de Physique des Interactions Ioniques et Moléculaires (PIIM), Marseille, France
e-mail: gregoire.danger@univ-amu.fr
[2] Ludwig-Maximilians-University, Department of Chemistry and Pharmacy, Butenandtstr. 5-13, 81377 Munich, Germany
e-mail: alexander.ruf@cup.uni-muenchen.de
[3] Helmholtz Zentrum München, Analytical BioGeoChemistry, Neuherberg, Germany
[4] Technische Universität München, Chair of Analytical Food Chemistry, Freising-Weihenstephan, Germany
[5] Centre de Recherche sur les Ions, les Matériaux et la Photonique (CEA/CNRS/ENSICAEN/UCBN), CIMAP, CIRIL, GANIL Caen, France
[6] Aix-Marseille Université, CNRS, CNES, LAM, Marseille, France
[7] Institut Universitaire de France (IUF), Paris, France

Received 27 April 2021 / Accepted 4 September 2021

ABSTRACT

Context. Sulfur (S) is of prime interest in the context of (astro)chemical evolution and habitability. However, the origin of S-bearing organic compounds in the Solar System is still not well constrained.
Aims. We carried out laboratory experiments to test whether complex organosulfur compounds can be formed when surfaces of icy Solar System bodies are subject to high-energy S ions.
Methods. Non-S-bearing organic residues, formed during the processing of astrophysical H_2O:CH_3OH:NH_3-bearing ice analogs, were irradiated with 105 keV-S^{7+} ions at 10 K and analyzed by high-resolving FT-ICR-MS. The resulting data were comprehensively analyzed, including network analysis tools.
Results. Out of several thousands of detected compounds, 16% contain at least one sulfur atom (organosulfur (CHNOS) compounds), as verified via isotopic fine structures. These residue-related organosulfur compounds are different from those formed during the S ion irradiation of ices at 10 K. Furthermore, insoluble, apolar material was formed during the sulfur irradiation of residues. Potential organosulfur precursors (CHNO molecules) were identified by means of molecular networks.
Conclusions. This evidence of organosulfur compounds formed by sulfur irradiation of organic residues sheds new light onto the rich and complex scope of pristine organosulfur chemistry in the Solar System, presented in the context of current and future space missions. These results indicate that the space weathering of Solar System bodies may lead to the formation of organosulfur compounds.

Key words. solid state: refractory – minor planets, asteroids: general – comets: general – methods: laboratory: molecular – astrochemistry – astrobiology

1. Introduction

Sulfur (S) represents one of the most interesting, albeit among the least understood, elements in the context of (astro)chemical evolution and habitability. Even though numerous sulfur-bearing molecules of increasing complexity have been detected in various astronomical environments, such as the CS in the ISM (Penzias et al. 1971), dense molecular clouds (Vastel et al. 2018), or protoplanetary disks (Le Gal et al. 2019) that include more complex species such as HCCSH and H_2CCS (McGuire et al. 2019), sulfur astrochemistry is far from being well constrained at present. One existing problem is the sulfur abundance in diffuse and dense astronomical environments. While in diffuse regions, the S abundance is close to the cosmic value (Neufeld et al. 2015; Sofia et al. 1994), diffuse regions are found to be depleted in sulfur (Jiménez-Escobar & Caro 2011; Prasad & Huntress Jr 1982). A possible solution to this problem could be that sulfur species might be locked in other forms than those that are routinely probed by observations. One suggestion is that sulfur is locked in the form of OCS in icy grain mantles (Palumbo et al. 1997) which would be in agreement with the absence of CS and the presence of COS/OCS on comet 67P/Churyumov-Gerasimenko (hereafter, comet 67P/C-G) (Rubin et al. 2019b). Furthermore, a recent modeling study suggests that most of the missing sulfur takes the form of organosulfur species trapped on grains (Laas & Caselli 2019).

Laboratory experiments have shown that the evolution of complex organic molecules can be simulated across various astrophysical environments, from dense molecular clouds to Solar System bodies such as comets (Herbst & van Dishoeck 2009; Öberg 2016; Fresneau et al. 2017; Gautier et al. 2020).

* Tables C.1 and C.2 are only available at the CDS via anonymous ftp to cdsarc.u-strasbg.fr (130.79.128.5) or via http://cdsarc.u-strasbg.fr/viz-bin/cat/J/A+A/655/A74

These experiments simulate the formation of astrophysical ices (e.g., including H_2O, CH_3OH, NH_3, CO, or CO_2) as observed in various environments (Boogert et al. 2015). These analogs are then submitted to irradiation, such as UV photons (Abou Mrad et al. 2016), X-ray radiation (Muñoz Caro et al. 2019), low-energy electrons (Abdulgalil et al. 2013) or ions (Ruf et al. 2019a), and subsequent thermal processing (Theulé et al. 2013).

Once at room temperature, an organic residue is formed that is usually soluble in polar solvents (water or methanol) and that can further evolve to insoluble material once irradiated (de Marcellus et al. 2017; Fresneau et al. 2017; Gautier et al. 2020). However, these simulation experiments mainly focus on CHNO-based molecular diversity but do not heavily account for organic sulfur chemistry (Mifsud et al. 2021). In this context, OCS has been discussed as a potential key molecule in sulfur chemical evolution (Palumbo et al. 1997). Furthermore, there is evidence that the irradiation of non-S-bearing ices (constituting H_2O, CH_3OH, and NH_3) with high-energy S^{7+} ions (at 105 keV) at 10 K leads to a rich and diverse organosulfur chemistry (Ruf et al. 2019a), indicating a complex organosulfur chemistry on S-irradiated icy body surfaces. Solar System bodies are abundant in refractory organic matter on their icy surfaces that can be further processed by ion implantation, as it is the case for comet 67P/C-G (Capaccioni et al. 2015). Space weathering alters the surface of Solar System bodies (Hapke 2001; Bennett et al. 2013). In this context, sulfur ions represent a significant source of irradiation within an energy range of 32 keV/ion (Von Steiger et al. 2000). Thus, the impact of sulfur irradiation of Solar System body surfaces might contribute to space weathering in the form of organosulfur compound formation.

In this study, we test whether organosulfur compounds can be formed when organic residues, laboratory analogs for Solar System body surfaces, are irradiated with S^{7+} (at 105 keV). Organic residues are formed by irradiating ices of H_2O:CH_3OH:NH_3 (2:1:1) with Ar^{7+} ions (at 105 keV), subsequently warmed to 300 K, and then irradiated by S^{7+} ions (at 105 keV) at 10 K again. The resulting residue (named "S^{7+}-over-irradiated residue") was probed for the formation of organosulfur compounds via high-resolving Electrospray Ionization Fourier Transform Ion Cyclotron Resonance Mass Spectrometry (ESI-FT-ICR-MS). The data were compared to a benchmark experiment which was performed with non-reactive Argon $(Ar)^{7+}$ ions (named "Ar^{7+}-irradiated ice"). The detection and chemical characterization of organosulfur molecules from S^{7+}-over-irradiated residues is discussed in comparison to S^{7+}-irradiated ices (named "S^{7+}-irradiated ice") and its astrophysical implications, with a particular focus on surfaces of Solar System objects.

2. Results and discussion

2.1. Detection of organosulfur (CHNOS) compounds in S^{7+}-over-irradiated residues

An organic residue was first formed by Ar^{7+}-irradiated ices (at 105 keV), composed of H_2O:CH_3OH:NH_3 (2:1:1) at 15 K. The processed ice was warmed up to 300 K and the resulting organic residue was then irradiated with S^{7+} ions (at 105 keV) at 10 K again. The resulting sample was probed for the presence of organosulfur species, and compared to the Ar^{7+}-irradiated ice sample.

Mass spectra from ESI-FT-ICR-MS analysis show similar features for the S^{7+}-over-irradiated residue and Ar^{7+}-irradiated ice residue with dense m/z signal patterns over a broad mass range (Fig. 1). Thanks to the high mass-resolving power and high mass accuracy (Ruf et al. 2017), FT-ICR-MS unambiguously revealed the detection of organosulfur (CHNOS) compounds in S^{7+}-over-irradiated residues. m/z signals that correspond to organosulfur (CHNOS) compounds were absent in the Ar^{7+}-irradiated ice. From 35 000 experimental m/z signals, ranging from 100 to 800 amu (atomic mass unit), 5822 C-, H-, N-, O-, or S-bearing molecular formulas could be unequivocally assigned in the S^{7+}-over-irradiated residue (5.3% CHO, 76.6% CHNO, 2.6% CHOS and 15.5% CHNOS, Fig. B.1, Table C.1, available in electronic form at the CDS), along with the m/z signals of both the global organic fingerprint and organosulfur (CHNOS) compounds, appear as regular patterns reflecting a chemosynthetic process as previously observed in UV-photon-irradiated ices (Danger et al. 2016; Fresneau et al. 2017; Gautier et al. 2020), ion-irradiated ices (Ruf et al. 2019a; Urso et al. 2020), or meteorites (Schmitt-Kopplin et al. 2010; Ruf et al. 2017, 2019c).

The presence of organosulfur (CHNOS) compounds has been validated by isotopic fine structure, enabled by FT-ICR-MS. Experimental mass spectra (dark-gray spectrum) have been compared to a molecule's theoretical simulated isotopic pattern at a natural abundance of C, H, N, O, and S (red spectrum), showing an excellent fit and thus confirming the presence of the tested molecule. Three examples of identified molecular ions, $[C_{22}H_{33}N_4O_3S]^-$ (Fig. 1), $[C_{21}H_{31}N_4O_3S]^-$ and $[C_{23}H_{35}N_6O_3S]^-$ (Fig. B.2) are presented.

On average, a stoichiometric formula of $C_{26}H_{38}N_6O_4S^-$ resulted (DBE= 10.5, H/C = 1.5, N/C = 0.2, O/C = 0.2, S/C = 0.05 and m/z = 532 amu). These CHNOS compounds are high mass molecules constituted with a high numbers of O and N atoms per molecule and bearing long carbon backbones. These result in depleted O/C and N/C ratios compared to ice-formed organosulfur (CHNOS) compounds (Figs. 2 and B.3). For both S^{7+}-over-irradiated residue and S^{7+}-irradiated ice, organosulfur (CHNOS) compounds bear mainly one S atom per molecule (93% bear one S atom for the S^{7+}-over-irradiated residue).

2.2. Differences between organosulfur (CHNOS) compounds formed on residues or inside ices

Organosulfur (CHNOS) compounds can be formed either by sulfur irradiation of astrophysical ices (Ruf et al. 2019a) or by the irradiation of organic residues (data presented here). The interaction of S ions in ices or with CHNO organic compounds in residues is significantly different.

Atomic ratio plots, known as a van Krevelen diagram (Van Krevelen 1950), were used to compare the detected organosulfur (CHNOS) compounds in irradiated residues and ice samples (non-irradiated residues). H/C against O/C representation enables a first screening of complex mixtures with respect to chemical families (Danger et al. 2016; Ruf et al. 2018; Schmitt-Kopplin et al. 2019). Organosulfur (CHNOS) compounds from S^{7+}-over-irradiated residues show a lower diversity in H/C, O/C and m/z compared to organosulfur (CHNOS) compounds formed in S^{7+}-irradiated ices (Figs. 2 and B.3) (Ruf et al. 2019a). The lower diversity in m/z features is also expressed by a single distribution found in #H-#C, #N-#C and #O-#C plots for over-irradiated residues, while these representations show two distinct patterns for residues generated from irradiated ices. Furthermore, the difference in diversity can be seen in CHNOS mass spectra and #N-#O plots. The irradiation of ices leads to the formation of precursor molecules which may include S atoms. In contrast, for irradiated organic residues, S directly interacts with larger complex

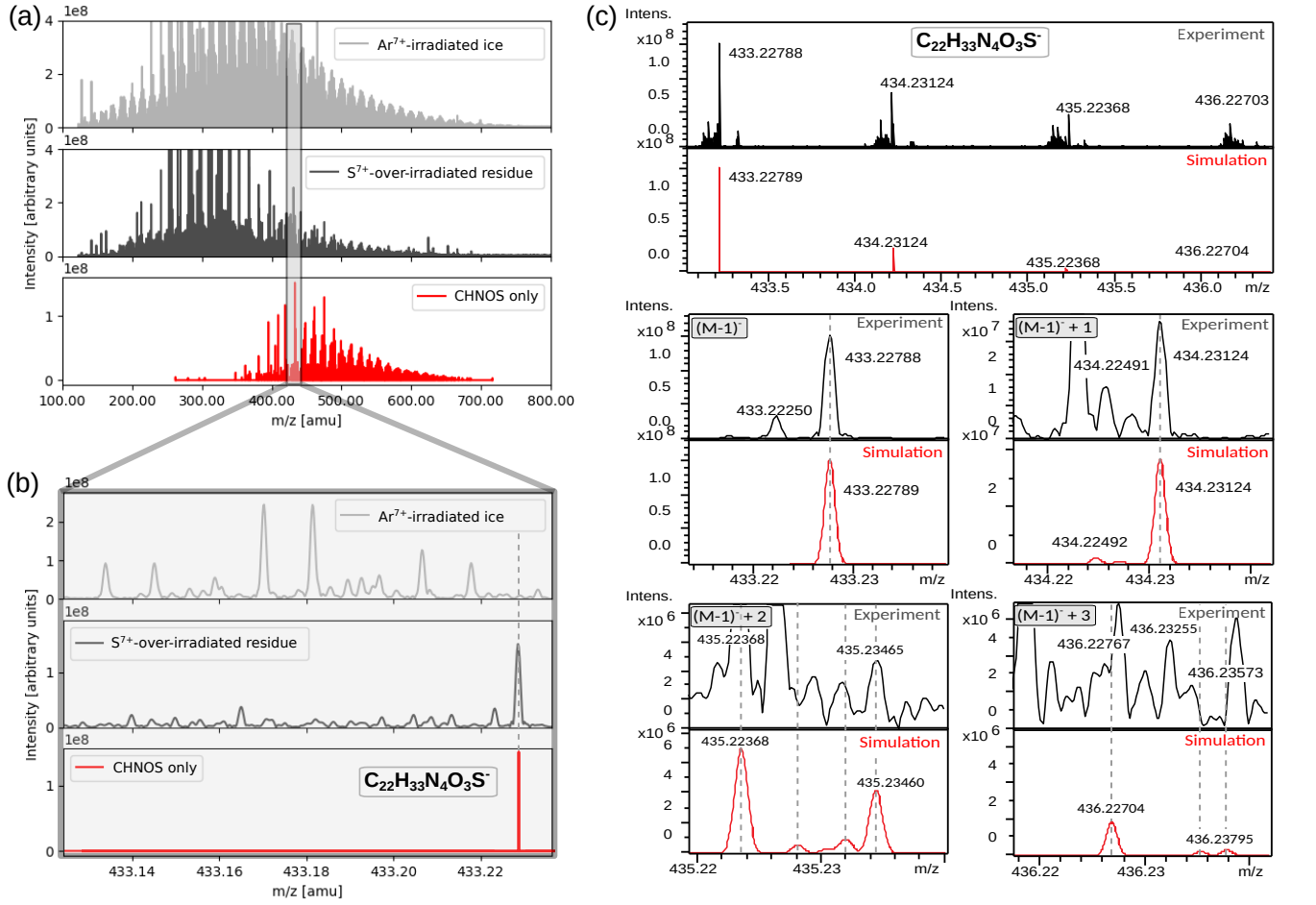

Fig. 1. Detection of organosulfur (CHNOS) compounds in S^{7+}-over-irradiated residues: (*a*, *b*) ESI-FT-ICR mass spectra enabled the detection of organosulfur (CHNOS) compounds in S^{7+}-over-irradiated residues (*2nd row*, darkgray). The "CHNOS-only" spectrum (*3rd row*, red) illustrates 908 CHNOS-assigned m/z signals that were absent in the Ar^{7+}-irradiated ice (reference sample, *1st row*, lightgray); (*c*) Organosulfur (CHNOS) compounds have been validated by isotopic fine structure as exemplarily shown for the $[C_{22}H_{33}N_4O_3S]^-$ molecular ion (darkgray = experimental spectrum, red = simulated isotopic pattern). Due to low intensities, $(M\text{-}1)^-$+2 and $(M\text{-}1)^-$+3 isotopologues are mixed with the noise signal.

organic molecules having already been formed, as indicated by the enrichment in molecular mass for organosulfur compounds in S^{7+}-over-irradiated residues compared to S^{7+}-irradiated ices (Fig. B.3).

The data provide evidence of depleted O/C ratios for CHNOS molecules in over-irradiated organic residues when compared to CHNOS-bearing ones detected in residues generated from irradiated ices. This oxygen depletion is also shown in the frequency distributions of atom counts. This is also in accordance with previous results from Gautier et al., offering evidence of decarboxylation reactions UV-over-irradiated organic residues (Gautier et al. 2020). These findings also match the previous results on the carbonization process among irradiated organic residues (loss of nitrogen and oxygen) (Jenniskens et al. 1993).

Furthermore, over-irradiated residues show also lower N/C and S/C ratios when compared to irradiated ices (Fig. B.3). However, this apparent depletion in N and S is explained by a high number of carbon atoms per molecular formula for over-irradiated residues. Absolute nitrogen and sulfur counts are similar for both over-irradiated and irradiated ice residues. The number of hydrogen atoms is also higher in over-irradiated residues. The significantly higher numbers of hydrogen and carbon atoms is supported by the higher m/z ratios found in the over-irradiated residue (Fig. 2).

Similarly to organic residues generated from irradiated ices (Ruf et al. 2019a), organosulfur (CHNOS) compounds from over-irradiated residues bear mostly one sulfur atom per molecular formula (Fig. B.3). The low number of multiple incorporated S atoms into organic molecules might be a result of small total amounts of sulfur implanted (Ruf et al. 2019a). However, there is the onset of S_2- and S_3- compounds for over-irradiated residues as compared to irradiated ices. This may indicate more efficient sulfur implantation for irradiated residues as S interacts here with larger molecules (organic matrix) whereas for ices, S interacts only with small molecules (CH_3OH, H_2O or NH_3), resulting in higher cross-sections for irradiated residues.

Residue-formed organosulfur (CHNOS) molecules have been found to be more unsaturated with higher masses than ice-formed ones. The DBE-#C plot illustrates that organosulfur (CHNOS) compounds formed by over-irradiated residues are enriched in carbon number and double bond equivalent (DBE) compared to organosulfur (CHNOS) molecules from residues generated from irradiated ices (black, Fig. 3). This finding is in accordance to H/C-, m/z-related data (Figs. 2 and B.3), concluding that residue-formed organosulfur (CHNOS) molecules are unsaturated with high masses.

When comparing both sets of organosulfur (CHNOS) molecules, the effect of residue irradiation might lead to the loss

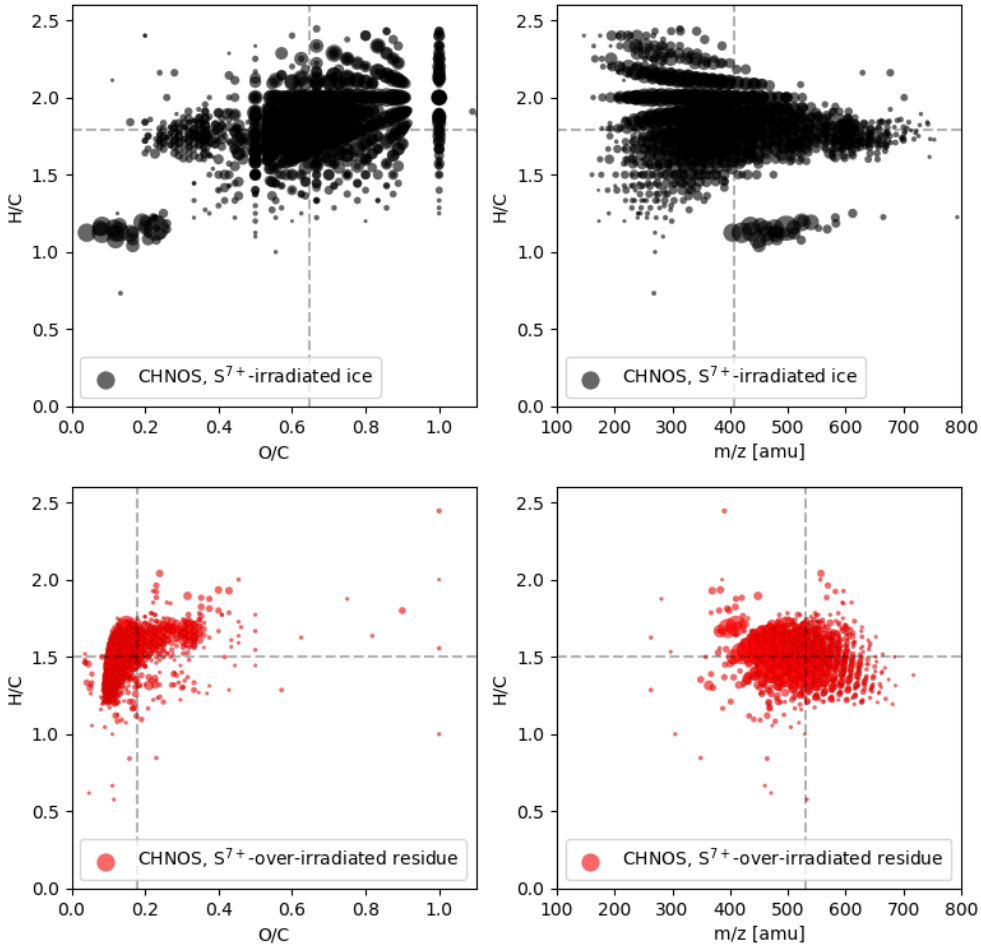

Fig. 2. Differences in heteroatoms and molecular mass for organosulfur (CHNOS) compounds formed on residues or inside ices. CHNOS compounds formed on S^{7+}-irradiated residues (red, *1st row*) have significantly lower O/C and higher molecular masses when compared to CHNOS compounds formed inside ices (black, *2nd row*).

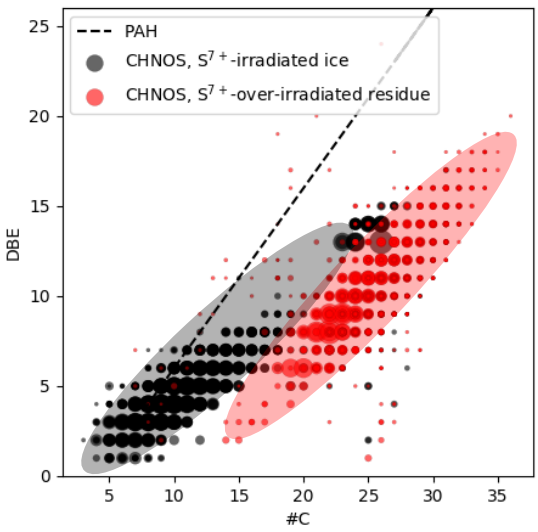

Fig. 3. Residue-formed organosulfur molecules (CHNOS) are more unsaturated than ice-formed ones. The DBE-#C plot illustrates that organosulfur (CHNOS) compounds formed by S^{7+}-over-irradiated residues are enriched in carbon number and double bond equivalent (DBE) CHNOS molecules formed inside S^{7+}-irradiated ices (black). For reference, characteristics of PAHs (polycyclic aromatic hydrocarbons, dashed line) are indicated.

of chemical functional groups (e.g., CO_2 Gautier et al. 2020). Furthermore, there might be a transition toward a more macromolecular network out of rather apolar organic molecules, as observed for the insoluble organic matter (IOM) in meteorites (Danger et al. 2021).

In addition to the methanol-soluble part of the over-irradiated residue sample, an apolar refractory part indeed remained that could not be dissolved in methanol, but in toluene instead. This "toluene fraction" is mainly composed of CHO molecules with high masses with low O/C ratios (Fig. B.4). The toluene fraction is characterized by apolar, saturated compounds (low DBEs) with high masses.

Overall, only one S atom per molecular formula has been observed for both residues (S^{7+}-over-irradiated residue and S^{7+}-irradiated ice), however, the characteristics of organosulfur (CHNOS) compounds are significantly different. This indicates multiple pathways in the molecules' synthesis. For irradiated ices at 10 K, only small molecules (e.g., CH_3OH) may interact with S atoms, governed by radical chemistry (recombination) and thermal reactivity during ice warm-up toward 300 K, resulting in a distribution of sulfur-bearing molecules in a broad mass range. For over-irradiated residues, complex organic molecules have been already formed before (during Ar irradiation at 10 K). Thus, the initial molecular substrate, to react with S ions, might be significantly different; S ions may then directly interact with a complex organic matrix resulting in S implantation on large

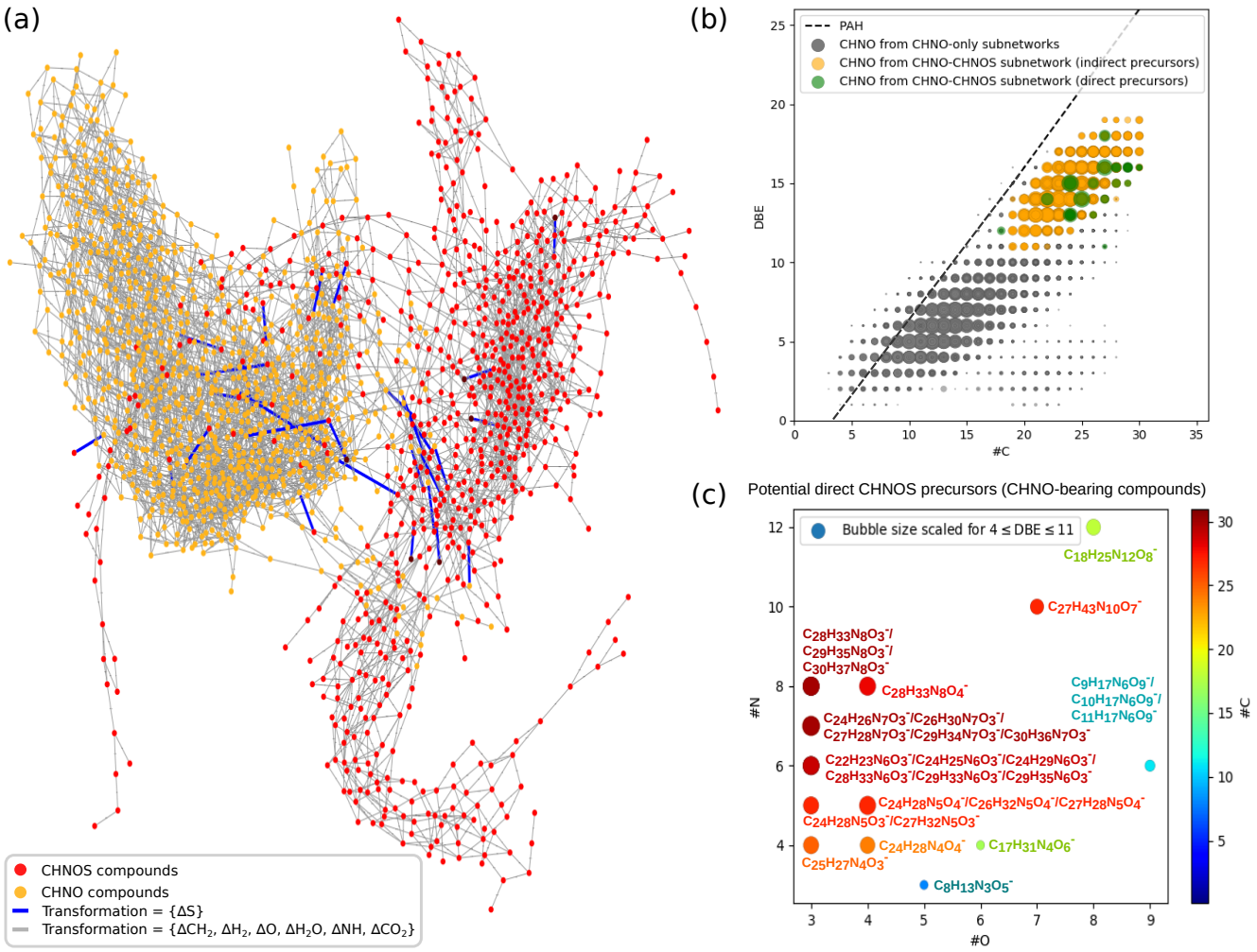

Fig. 4. CHNO-CHNOS molecular network: (*a*) molecular network of 1669 molecular formulas (orange nodes = CHNO compounds, from Ar^{7+}-irradiated ice + red nodes = CHNOS compounds, from S^{7+}-over-irradiated residue) illustrates the potential transformation of CHNO compounds toward CHNOS ones. Gray edges represent ΔCH_2, ΔH_2, ΔO, ΔH_2O, ΔNH and ΔCO_2, while ΔS transformations are shown in blue; (*b*) potential CHNOS precursors are significantly enriched in carbon number and double bond equivalent (DBE) compared to CHNO compounds that are not part of the CHNO-CHNOS molecular network. For reference, characteristics of PAHs (polycyclic aromatic hydrocarbons, dashed line) are indicated; (*c*) 29 potential direct CHNOS precursors (connected by ΔS transformations) show high N and C counts while having moderate numbers of O atoms per molecular formula (#N-#O-#C plot with bubble size scaled for $4 \leq DBE \leq 11$).

complex organic molecules or in molecular recombination due to the energy impact, while in ice, S mainly interacts with water.

2.3. CHNO-CHNOS molecular network

A molecular network analysis has been used to examine if the complex CHNO chemical family (formed during Ar^{7+}-irradiation of H_2O:CH_3OH:NH_3 ices, step 1) is connected to CHNOS molecules (formed during S^{7+}-over-irradiation of formed organic residues, step 2, see details in Appendix A) via a ΔS transformation. Here, CHNO represents the major chemical family for over-irradiated residues (Fig. B.1) but also for UV-irradiated (Danger et al. 2016), Ar^{7+} and S^{7+}-irradiated ices (Ruf et al. 2019a), and H^+-irradiated ices (Urso et al. 2020). These findings indicate that CHNO compounds might likely form in a universal process of irradiated ices via radical chemistry, independent of the irradiation source itself (Butscher et al. 2017; Theulé et al. 2013). Molecular networks were set-up using the union of CHNO (Ar^{7+}-irradiated ice data) and CHNOS (S^{7+}-over-irradiated residue data) sets as nodes of the network, while the transformations ΔCH_2, ΔH_2, ΔO, ΔH_2O, ΔNH, ΔCO_2, ΔS represent the edges. Here, ΔCH_2, ΔH_2, ΔO, ΔH_2O, ΔNH, ΔCO_2 represent potential reactions building up homologous series of a chemical family (gray edges), while ΔS (blue edges) illustrates possible sulfur implantation happening during S ion irradiation process on an organic residue (Fig. 4).

A subnetwork of 1669 molecular formulas has been identified which connects CHNO (orange nodes) with CHNOS species (red nodes), and represents the 3rd largest component out of 53 components in total for the whole data set (18% coverage of all nodes in the complete molecular network, Fig. B.5). The CHNO-CHNOS molecular network is constituted of 920 CHNO compounds (55%) and 749 CHNOS compounds (45%). These CHNO molecules represent potential CHNOS precursors, either directly (reacting with S atoms toward CHNOS molecules, referred to as "potential direct CHNOS precursors") or indirectly (reacting with non-S-bearing molecules, e.g., H_2 or CO_2, referred to as "potential indirect CHNOS precursors"). The network out of 18% of all detected CHNO and CHNOS that have been identified illustrates the potential transformation

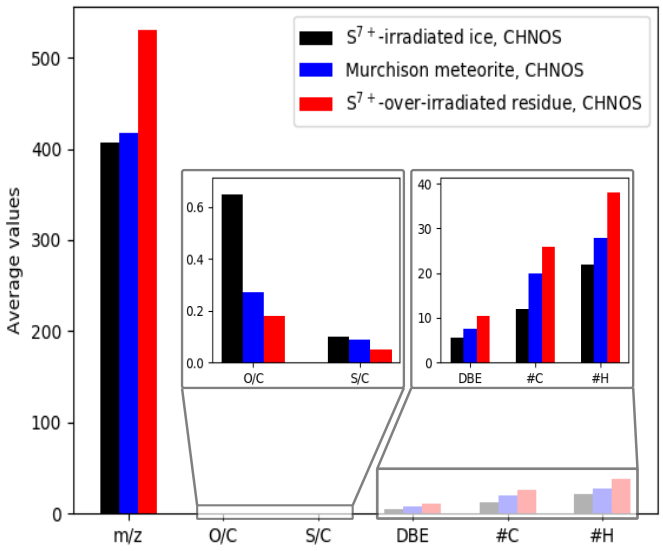

Fig. 5. Relationship between organosulfur compounds (CHNOS) from S^{7+}-irradiated ices, Murchison meteorite and S^{7+}-over-irradiated residues.

of CHNO molecules to organosulfur (CHNOS) ones, but also describes the unique characteristics of specific CHNO compounds that are named "potential direct CHNOS precursors". These potential direct CHNOS precursors were mostly absent in S^{7+}-over-irradiated residues.

Potential CHNOS precursors (CHNO-bearing compounds) have significant chemical differences compared to CHNO compounds which are not part of the CHNO-CHNOS molecular network (Fig. B.6). Enriched carbon numbers and double bond equivalents (DBE) have been observed for CHNO molecules connected with the organosulfur (CHNOS) chemical family. Furthermore, a lesser extent of chemical diversity has been observed for CHNO compounds connected to CHNOS species (Fig. B.6). Depletion in O/C, N/C, H/C, as well as specific enrichments of #H, #C, and molecular mass, have been observed (Figs. 2, B.3, and B.6). Thus, 29 potential direct CHNOS precursors (connected by ΔS transformations) show high N and C counts while having moderate numbers of O atoms per molecular formula (Fig. 4, Table C.2 – available in electronic form at the CDS).

These findings offer detailed evidence that CHNO compounds react very selectively with irradiated sulfur atoms to form organosulfur compounds. The CHNO and CHNOS chemistry is in major part related within their chemical families (e.g. within CHNO species only) but the transition between different chemical families (e.g., CHNO species → CHNOS species) is very specific, as indicated by the low number of direct ΔS transitions.

2.4. Relationship with the Murchison meteorite

Organosulfur compounds have been found to be key in the chemical evolution of meteorites. Next to organomagnesium (Ruf et al. 2017), organosulfur compounds (Schmitt-Kopplin et al. 2010; Popova et al. 2013; Bartoschewitz et al. 2017; Ruf et al. 2018) play an important role in the description of chemical evolution of meteorites (e.g., the thermal history).

Organosulfur (CHNOS) characteristics of the Murchison meteorite were found to be in between of those from S^{7+}-irradiated ices and S^{7+}-over-irradiated residues (Figs. 5 and B.7). Monitoring m/z, DBE, #C and #H, an increase from ice (CHNOS) over Murchison (CHNOS) to residue (CHNOS) has been observed. The effect is reversed for heteroatom ratios O/C and S/C.

This indicates that the organosulfur chemistry of Murchison does not only reflect the complex secondary processing of organic matter (e.g., water-rock interactions, aqueous alteration including minerals) but may also observe a primordial signature on the part of mixed irradiated ice and surface processes for astrophysical objects (Vinogradoff et al. 2018; Ruf et al. 2019b; Danger et al. 2021).

3. Astrophysical implications

The data presented here demonstrate evidence that complex organosulfur molecules, next to insoluble material, might be formed on astrophysical surfaces, which are exposed to highly energetic S ions, as this might be the case for surfaces on Solar System bodies. This implies that during space weathering, sulfur might be trapped in the form of complex organosulfur molecules not only inside cold irradiated astrophysical ices (Ruf et al. 2019a) but also on ion-irradiated surfaces of icy bodies, such as icy moons.

A variety of objects of our Solar System present a notable amount of refractory organic matter on their surfaces, exposed to an influx of sulfur ions, possibly triggering organosulfur chemistry similar to that observed in our laboratory experiments. Regarding the source of sulfur radiation in the Solar System, the Solar wind provides a modest but steady source of sulfur ions at energies comparable to those applied in our laboratory experiments (32 keV ion^{-1} for the 400 km s^{-1} Solar wind) (Von Steiger et al. 2000). The Jovian magnetosphere features a large amount of sulfur ions, having energies up to a few hundreds of keV (Allen et al. 2019). We go on to discuss possible relations to asteroids of the main belt (Ceres), giant planet icy moons, comets, and Kuiper belt objects.

3.1. Main belt asteroids (and Ceres)

Asteroids of the main belt may represent various candidate environments in which organic compounds might have reacted with sulfur at different stages of evolution.

Due to the brief persistence of water at this distance from the sun, this type of organic matter would be a relevant parallel to our laboratory irradiation experiments on organic residues that have lost their volatile compounds. Based on measurements of the solar wind, O flux, and S/O ratio (Von Steiger et al. 2000, 2010) we evaluate the sulfur flux at 2.8 AU (the position of Ceres) to be 6×10^2 ions cm^{-2} s^{-1}. Therefore, a surface at this distance would receive the same sulfur fluence as in our experiments for about 12 000 yr.

Due to their spectral similarity, carbonaceous chondrites, and C-type asteroids are suspected to be related to each other and might therefore be similar in their amounts of organic matter (Martins et al. 2020). Attributed features to organic compounds have been detected for some asteroids (Cruikshank & Brown 1987; Campins et al. 2010; Rivkin & Emery 2010; Licandro et al. 2011). These are mostly in the 3–3.6 microns region that is often not covered in ground-based observations of asteroids. Rivkin and Emery suggested the presence of tholins as a result of water and ethane irradiation and a mixture of polycyclic hydrocarbons, in addition to abundant amorphous carbon (Rivkin & Emery 2010). However, a more detailed and better

constrained characterization of these materials might be obtained by sample returns. An analysis of grains brought from asteroid Itokawa by the Hayabusa mission showed the presence of organic matter being rich in polyaromatic hydrocarbons and heavily graphitized organic molecules (Chan et al. 2021). The analysis of samples returned by the Hayabusa 2 (Watanabe et al. 2017) and OSIRIS-REX missions (Lauretta et al. 2017), from C-type asteroids (162173 Ryugu and 101955 Bennu, respectively) will significantly enhance the level of available information on the organic material present on asteroids' surfaces and might also enable the exploration of their organosulfur chemistry. Future space-based observations including the *James Webb* Space Telescope (JWST) will enable a better investigation of a large collection of objects, including asteroids as well as Trans-Neptunian objects.

The surface of dwarf planet Ceres has shown some areas, mainly around the Ernutet Crater, to be enriched in aliphatic organic compounds (De Sanctis et al. 2017), potentially including amine-type molecules. This type of organic matter is poor in aromatic compounds and in oxygen functions (below 20–30 wt%) (De Sanctis et al. 2019). Locally, the organic content of the surface appears larger than in carbonaceous chondrites, with spectral matches between mixtures including 4–9 wt% aliphatic compounds (De Sanctis et al. 2017). This type of organic matter might have been exposed to sulfur irradiation (from the Solar wind) for a short amount of time (Bowling et al. 2020).

3.2. Icy moons of giant planets

In the Jovian system, where the magnetosphere offers an intense source of sulfur ion irradiations, organic matter is likely present, although the amounts and characteristics are unclear. Europa, as the most exposed Galilean icy satellites, receives up to 9.7×10^7 sulfur ions cm^{-2} s^{-1} on parts of its trailing hemisphere (Dalton III et al. 2013). The bulk of these sulfur ions has an energy between a few 10 keV up to 1 MeV (Cooper et al. 2001). The sulfur fluence received by our sample ($\approx 5 \times 10^{14}$ sulfur ions cm^{-2}) during over-irradiation is related to less than five months on the most intensely irradiated regions of Europa. Ganymede and Callisto receive a lower sulfur flux, by one to more than two orders of magnitude depending on the region considered (Cooper et al. 2001).

The amount of hydrocarbons on Europa's surface (Jupiter moon) seems limited (Carlson et al. 2009), since the aliphatic CH band could not be detected. Hydrocarbons might still be delivered to Europa's surface by (micro)meteoritic impacts but they could be present in small amounts and buried in ice, making water-organic-based radiation chemistry all the more relevant. The CO_2 detected on Europa may be a result of the radiolytic degradation of this type of organic material. Emplacements of complex organics on the surface from the ocean could also occur thanks to putative geysers (Roth et al. 2014; Sparks et al. 2016; Jia et al. 2018) and these organics would then be exposed to sulfur implantation.

On two other Jupiter moons, Ganymede and Callisto, the IR detection of organic molecules has been reported, with likely low amounts of C-H and C-N containing molecules and tholins (McCord et al. 1997). Future observations by space missions (the Juno extended mission (Bolton et al. 2017), and the Europa Clipper (Phillips & Pappalardo 2014) and JUICE (Grasset et al. 2013 spacecrafts) will bring more constraints as to the presence of organic compounds on the surface of these moons through IR observation of the surfaces. Detection of organosulfur through the onboard infrared spectrometers is a more remote possibility due to the paucity of low-temperature spectral data for this category of compounds. Thiol ices do show characteristic features in the mid IR (Hudson & Gerakines 2018) but the low quantity of sulfur in our experiments did not allow for IR detection of these compounds, if they were formed. Onboard mass spectrometers (Europa Clipper's MASPEX and SUDA, JUICE's PEP) may be able to detect refractory organic matter sputtered from the surface, including matter that went through sulfur implantation.

Satellites of Saturn, Phoebe and Iapetus, show high amounts of refractory organics on their surfaces, including features attributed to PAHs (polycyclic aromatic hydrocarbons) and aliphatic compounds (Cruikshank et al. 2008). While the magnetosphere of Saturn is low in density of sulfur ions, Phoebe is suspected to be a captured object (by Saturn) (Clark et al. 2019) and is thus expected to have had significant exposure times to the solar wind (and thus to sulfur ions).

On Saturn's moon Enceladus, the outflow of various macromolecular organic compounds by geysers (Postberg et al. 2018) indicates that in other active icy bodies, organics coming from their interior oceans would be exposed to sulfur irradiation on their surfaces.

3.3. Comets

Comets are most likely rich in organic matter, including refractory organic matter that could have undergone sulfur implantation. Results from the Rosetta mission to comet 67P/Chuyrumov-Gerasimenko (comet 67P/C-G) report a rich presence of both semi-volatile and refractory organic compounds (Filacchione et al. 2019; Rubin et al. 2019a, 2020), including aliphatic (Altwegg et al. 2017; Raponi et al. 2020) and polyaromatic compounds (Quirico et al. 2016). An analysis of comet 67P/C-G's dust reports up to 50 wt% organic matter (Bardyn et al. 2017). Implantation of sulfur ions into such cometary organic material would present similarities with our experimental conditions, especially since laboratory residues from cometary ice analogs have been found to spectrally match with this refractory material, with the putative presence of carboxylic compounds (Quirico et al. 2016). Due to its refractory characteristics, these type of organics might be mostly preserved during the comet's activity and may witness the organic chemistry triggered by the Solar wind. Sulfur-bearing organics have been reported in samples of the semi-volatile phase analyzed by the onboard mass spectrometers of the Rosetta spacecraft and the Philae lander, including CHS, CH_2S, C_2H_6S, C_2H_2S (Altwegg et al. 2017). This supports the possibility that sulfur might be also present in the comet's refractory organic phase. Analyses of comet 67P's refractory organic matter indicate a H/C ratio of around 1 (Isnard et al. 2019), which is consistent with more intense radiation than in our laboratory experiments.

Results from the Cometary and Interstellar Dust Analyzer on the Stardust spacecraft revealed the presence of abundant organic matter in dust grains of comet 81P/Wild 2 (Kissel et al. 2004). This organic material might be present in aromatic compounds and SH-ions, and putatively includes organosulfur species. The presence of abundant organic matter, mostly aromatic-type material, has been inferred on dust grains of comet 1P/Halley Kissel & Krueger (1987). CHNO compounds were found to be abundant in the dust grains of comet 1P/Halley (Mitchell et al. 1992; Fomenkova et al. 1994) and 81P/Wild 2 (Kissel et al. 2004). The organic matter of comet 67P/C-G appears to be depleted in nitrogen with respect to the composition of other comets (Capaccioni et al. 2015; Altwegg et al. 2017).

3.4. Kuiper belt objects (KBOs)

In terms of temperature, Kuiper Belt Objects (KBOs) show the closest parallel to our laboratory experiments. The surface of the dwarf planet Pluto shows the presence of dark materials, likely due to deposition of atmospheric haze material (Grundy et al. 2018), and red-colored regions that could signal complex organic molecules being exposed to various energetic processes (e.g., radiation from the solar wind). In any case, the estimated high rates of deposition, combined with Pluto's atmosphere preventing lowest-energy particle reaching the surface, ensures that radiolytic processing would be minor.

Pluto's satellite Charon indicates the presence of ammoniated material (Grundy et al. 2016) and orange-colored material potentially assigned as a result of methane photolysis. On the Kuiper-Belt object Arrokoth, red-and-orange-colored spots have been observed on its surface which have been assigned to complex macromolecular organic material (Cruikshank et al. 2020), likely resulting from methanol radiolysis and photolysis on the surface (Grundy et al. 2020). This would represent a good target for sulfur implantation and the subsequent formation of organosulfur compounds. The low amounts of water on Arrokoth's surface (or its lack overall Grundy et al. 2020), is in agreement with our experimental conditions.

In summary, even though the details between Solar System objects and our experimental laboratory conditions may vary, many objects in the Solar System represent ideal candidates for studies of sulfur implantation into organic matter; potentially unveiling key insights into locked sulfur in the form of complex organosulfur compounds.

4. Conclusions

We investigated the formation of complex organosulfur compounds on simulated surfaces of Solar System bodies irradiated by high-energy sulfur ions. Our main findings are summarized below:

1. High-resolving FT-ICR-MS analysis enabled the detection of many hundreds of organosulfur (CHNOS) compounds (16% of totally many thousand detected compounds) in S^{7+}-over-irradiated residues originating from H_2O:CH_3OH:NH_3 ices (CHNOS compounds were absent in Ar^{7+}-irradiated reference samples; validation via isotopic fine structure).
2. Surface-formed organosulfur compounds are found to be different compared to organosulfur compounds formed directly inside respective astrophysical ices (depletion in O/C, N/C, S/C; enrichment in molecular mass, #C, #H).
3. Using a molecular network analysis, potential CHNOS organic precursors (CHNO-bearing molecules) are identified and found to have different properties compared to CHNO molecules that are not linked to organosulfur compounds. Direct precursor molecules (linked via ΔS with CHNOS compounds) constitute multiple nitrogen atoms per molecular formula.
4. Organosulfur (CHNOS) characteristics of the Murchison meteorite were found to be in between of those from S^{7+}-irradiated ices and S^{7+}-over-irradiated residues.
5. Formed organosulfur molecules on simulated S-irradiated icy surfaces, including insoluble and apolar material, indicates that there should be a significant amount of sulfur-bearing material in respective Solar System bodies, a finding that sheds new light onto the problem of locked sulfur in the astrophysical context.

Acknowledgements. A.R., G.D. and A.B. thank Centre National d'Etudes Spatiales for funding (CNES Postdoctoral Fellowship 2018 & 2020). The research was funded with support from the Centre National d'Etudes Spatiales (CNES, R-S18/SU-0003-072 and R-S18/SU-0003-072, PI: G. D.), and the Centre National de la Recherche Française (CNRS) with the programs "Physique et Chimie du Milieu Interstellaire" (PCMI-PI: G.D.) and "Programme National de Planétologie" (PNP) (PI: G.D. and L.D. H.). G.D is grateful to the Agence nationale de la recherche for funding via ANR RAHIIA_SSOM (Projet-ANR-16-CE29-0015). P.S-K. thank the Deutsche Forschungsgemeinschaft (DFG, German Research Foundation) - Project-ID 364653263 - TRR 235 for their funding. P.B. thanks the Agence nationale de la recherche for funding via ANR IGLIAS (Projet-ANR-13-BS05-0004).

References

Abdulgalil, A. G. M., Marchione, D., Thrower, J., et al. 2013, Phil. Trans. R. Soc. A Math. Phys. Eng. Sci., 371, 20110586
Abou Mrad, N., Duvernay, F., Chiavassa, T., & Danger, G. 2016, MNRAS, 458, 1234
Allen, R., Paranicas, C., Bagenal, F., et al. 2019, Geophys. Res. Lett., 46, 11709
Altwegg, K., Balsiger, H., Berthelier, J.-J., et al. 2017, MNRAS, 469, S130
Augé, B., Been, T., Boduch, P., et al. 2018, Rev. Sci. Instrum., 89, 075105
Bardyn, A., Baklouti, D., Cottin, H., et al. 2017, MNRAS, 469, S712
Bartoschewitz, R., Appel, P., Barrat, J.-A., et al. 2017, Geochemistry, 77, 207
Bennett, C. J., Pirim, C., & Orlando, T. M. 2013, Chem. Rev., 113, 9086
Bolton, S., Lunine, J., Stevenson, D., et al. 2017, Space Sci. Rev., 213, 5
Boogert, A. A., Gerakines, P. A., & Whittet, D. C. 2015, ARA&A, 53, 541
Bowling, T. J., Johnson, B. C., Marchi, S., et al. 2020, Earth Planet. Sci. Lett., 534, 116069
Butscher, T., Duvernay, F., Rimola, A., Segado-Centellas, M., & Chiavassa, T. 2017, Phys. Chem. Chem. Phys., 19, 2857
Campins, H., Hargrove, K., Pinilla-Alonso, N., et al. 2010, Nature, 464, 1320
Capaccioni, F., Coradini, A., Filacchione, G., et al. 2015, Science, 347, 6220
Carlson, R., Calvin, W., Dalton, J., et al. 2009, Europa (Tucson: University of Arizona Press), 283
Chan, Q., Stephant, A., Franchi, I., et al. 2021, Sci. Rep., 11, 1
Clark, R. N., Brown, R. H., Cruikshank, D. P., & Swayze, G. A. 2019, Icarus, 321, 791
Cooper, J. F., Johnson, R. E., Mauk, B. H., Garrett, H. B., & Gehrels, N. 2001, Icarus, 149, 133
Cruikshank, D., & Brown, R. H. 1987, Science, 238, 183
Cruikshank, D. P., Wegryn, E., Dalle Ore, C. M., et al. 2008, Icarus, 193, 334
Cruikshank, D. P., Pendleton, Y. J., & Grundy, W. M. 2020, Life, 10, 126
Dalton III, J., Cassidy, T., Paranicas, C., et al. 2013, Planet. Space Sci., 77, 45
Danger, G., Orthous-Daunay, F.-R., de Marcellus, P., et al. 2013, Geochim. Cosmochim. Acta, 118, 184
Danger, G., Fresneau, A., Mrad, N. A., et al. 2016, Geochim. Cosmochim. Acta, 189, 184
Danger, G., Ruf, A., Maillard, J., et al. 2020, Planet. Sci. J., 1, 55
Danger, G., Vinogradoff, V., Matzka, M., et al. 2021, Nat. Commun., 12, 1
de Marcellus, P., Meinert, C., Myrgorodska, I., et al. 2015, Proc. Natl. Acad. Sci., 112, 965
de Marcellus, P., Fresneau, A., Brunetto, R., et al. 2017, MNRAS, 464, 114
De Sanctis, M. C., Ammannito, E., McSween, H. Y., et al. 2017, Science, 355, 719
De Sanctis, M. C., Vinogradoff, V., Raponi, A., et al. 2019, MNRAS, 482, 2407
Filacchione, G., Groussin, O., Herny, C., et al. 2019, Space Sci. Rev., 215, 1
Fomenkova, M., Chang, S., & Mukhin, L. 1994, Geochim. Cosmochim. Acta, 58, 4503
Fresneau, A., Abou Mrad, N., d'Hendecourt, L. L., et al. 2017, ApJ, 837, 168
Gautier, T., Danger, G., Mousis, O., et al. 2020, Earth Planet. Sci. Lett., 531, 116011
Grasset, O., Dougherty, M., Coustenis, A., et al. 2013, Planet. Space Sci., 78, 1
Grundy, W., Binzel, R., Buratti, B., et al. 2016, Science, 351, aad9189
Grundy, W. M., Bertrand, T., Binzel, R. P., et al. 2018, Icarus, 314, 232
Grundy, W. M., Bird, M. K., Britt, D. T., et al. 2020, Science, 367, eaay3705
Hapke, B. 2001, J. Geophys. Res. Planets, 106, 10039
Herbst, E., & van Dishoeck, E. F. 2009, ARA&A, 47, 427
Hudson, R. L., & Gerakines, P. A. 2018, ApJ, 867, 138
Isnard, R., Bardyn, A., Fray, N., et al. 2019, A&A, 630, A27
Jenniskens, P., Baratta, G. A., Kouchi, A., et al. 1993, A&A, 273, 583
Jia, X., Kivelson, M. G., Khurana, K. K., & Kurth, W. S. 2018, Nat. Astron., 2, 459

Jiménez-Escobar, A., & Caro, G. M. 2011, A&A, 536, A91
Kissel, J., & Krueger, F. 1987, Nature, 326, 755
Kissel, J., Krueger, F. R., Silén, J., & Clark, B. C. 2004, Science, 304, 1774
Laas, J. C., & Caselli, P. 2019, A&A, 624, A108
Lauretta, D. S., Balram-Knutson, S. S., Beshore, E., et al. 2017, Space Sci. Rev., 212, 925
Le Gal, R., Öberg, K. I., Loomis, R. A., Pegues, J., & Bergner, J. B. 2019, ApJ, 876, 72
Licandro, J., Campins, H., Kelley, M., et al. 2011, A&A, 525, A34
Lv, X., de Barros, A., Boduch, P., et al. 2012, A&A, 546, A81
Martins, Z., Chan, Q. H. S., Bonal, L., King, A., & Yabuta, H. 2020, Space Sci. Rev., 216, 1
McCord, T. a., Carlson, R. W., Smythe, W. D., et al. 1997, Science, 278, 271
McGuire, B. A., Shingledecker, C. N., Willis, E. R., et al. 2019, ApJ, 883, 201
Mifsud, D. V., Kaňuchová, Z., Herczku, P., et al. 2021, Space Sci. Rev., 217, 14
Mitchell, D., Lin, R., Carlson, C., et al. 1992, Icarus, 98, 125
Muñoz Caro, G. M., Ciaravella, A., Jimenez-Escobar, A., et al. 2019, ACS Earth and Space Chemistry (Washington: ACS Publications)
Neufeld, D., Godard, B., Gerin, M., et al. 2015, A&A, 577, A49
Öberg, K. I. 2016, Chem. Rev., 116, 9631
Palumbo, M., Geballe, T., & Tielens, A. G. 1997, ApJ, 479, 839
Penzias, A., Solomon, P., Wilson, R., & Jefferts, K. 1971, ApJ, 168, L53
Phillips, C. B., & Pappalardo, R. T. 2014, Eos, Trans. Am. Geophys. Union, 95, 165
Popova, O. P., Jenniskens, P., Emel'yanenko, V., et al. 2013, Science, 342, 1069
Postberg, F., Khawaja, N., Abel, B., et al. 2018, Nature, 558, 564
Prasad, S. S., & Huntress Jr, W. T. 1982, ApJ, 260, 590
Quirico, E., Moroz, L., Schmitt, B., et al. 2016, Icarus, 272, 32
Raponi, A., Ciarniello, M., Capaccioni, F., et al. 2020, Nat. Astron., 4, 500
Rivkin, A. S., & Emery, J. P. 2010, Nature, 464, 1322
Roth, L., Saur, J., Retherford, K. D., et al. 2014, Science, 343, 171
Rubin, M., Altwegg, K., Balsiger, H., et al. 2019a, MNRAS, 489, 594
Rubin, M., Bekaert, D. V., Broadley, M. W., Drozdovskaya, M. N., & Wampfler, S. F. 2019b, ACS Earth Space Chem., 3, 1792
Rubin, M., Engrand, C., Snodgrass, C., et al. 2020, Space Sci. Rev., 216, 1
Ruf, A., Kanawati, B., Hertkorn, N., et al. 2017, PNAS, 114, 2819
Ruf, A., D'Hendecourt, L. L. S., & Schmitt-Kopplin, P. 2018, Life, 8, 18
Ruf, A., Bouquet, A., Boduch, P., et al. 2019a, ApJ, 885, L40
Ruf, A., Lange, J., Eddhif, B., et al. 2019b, ApJ, 887, L31
Ruf, A., Poinot, P., Geffroy, C., Le Sergeant d'Hendecourt, L., & Danger, G. 2019c, Life, 9, 35
Schmitt-Kopplin, P., Gabelica, Z., Gougeon, R. D., et al. 2010, PNAS, 107, 2763
Schmitt-Kopplin, P., Hemmler, D., Moritz, F., et al. 2019, Faraday Discuss, 218, 9
Senior, J. K. 1951, Am. J. Math., 73, 663
Shannon, P., Markiel, A., Ozier, O., et al. 2003, Genome Res., 13, 2498
Sofia, U. J., Cardelli, J. A., & Savage, B. D. 1994, ApJ, 430, 650
Sparks, W. B., Hand, K., McGrath, M., et al. 2016, ApJ, 829, 121
Theulé, P., Duvernay, F., Danger, G., et al. 2013, Adv. Space Res., 52, 1567
Tziotis, D., Hertkorn, N., & Schmitt-Kopplin, P. 2011, Euro. J. Mass Spectr., 17, 415
Urso, R. G., Vuitton, V., Danger, G., et al. 2020, A&A, 644, A115
Van Krevelen, D. 1950, Fuel, 29, 269
Van Rossum, G., & Drake Jr, F. L. 1995, Python tutorial, 620 (Centrum voor Wiskunde en Informatica Amsterdam)
Vastel, C., Quénard, D., Le Gal, R., et al. 2018, MNRAS, 478, 5514
Vinogradoff, V., Bernard, S., Le Guillou, C., & Remusat, L. 2018, Icarus, 305, 358
Von Steiger, R., Schwadron, N., Fisk, L., et al. 2000, J. Geophys. Res. Space Phys., 105, 27217
Von Steiger, R., Zurbuchen, T. H., & McComas, D. J. 2010, Geophys. Res. Lett., 37, L22101
Watanabe, S.-i., Tsuda, Y., Yoshikawa, M., et al. 2017, Space Sci. Rev., 208, 3
Ziegler, J. F., Ziegler, M. D., & Biersack, J. P. 2010, Nucl. Instrum. Methods Phys. Res. Sect. B, 268, 1818

Appendix A: Methods

Appendix A.1: Formation of ion-irradiated and ion-over-irradiated residues from astrophysical ice analogs

The ion beam used for irradiation was generated at the ARIBE low-energy line of the Grand Accélérateur National d'Ions Lourds (GANIL) Large Heavy Ion National Accelerator facilities in Caen, France. For both Ar^{7+} and S^{7+}, the ion beam was formed by ions at an energy of 105 keV/ion, with a flux of ≈1 x 10^{11} cm^{-2} s^{-1}. A mobile Faraday cup enabled a measurement of the intensity of the ion beam and prevented the beam from reaching the targets when needed. The main vacuum chamber contained three windows out of ZnSe to be cooled down to minimally 9 K and holding one sample each. Windows were kept at 10 K during deposition and irradiation. Ice samples were formed by preparing a gas mixture in a premixing chamber and depositing this vapor using a mobile needle, allowing targeted deposition onto a desired window. This device effectively enabled the generation and irradiation of three different deposited samples at similar vacuum conditions. Details on beam generation (Lv et al. 2012) and the IGLIAS device (Augé et al. 2018) have been described previously.

Using an initial gas mixture of H_2O:CH_3OH:NH_3 = 2:1:1 for the S^{7+}-over-irradiated residue, S^{7+}-irradiated ice and Ar^{7+}-irradiated ice samples, ices and their corresponding residues were formed. To maximize the yield of formed residues, several layers were deposited for each sample. A new layer was deposited when the underlying irradiated layer had reached steady state conditions. Each layer was subsequently deposited and irradiated (deposit of 1 layer corresponded to 1mbar / 1 μm; irradiation for 30 minutes; then the next layer was deposited). In total, 15 layers were formed for the Ar^{7+}-irradiated ice and 19 layers for the sulfur-over-irradiated residue (S^{7+} ions). The deposited quantity roughly corresponds to 0.5 μm, which is thicker than the penetration depths of 105 keV per S^{7+} or Ar^{7+}, calculated to be <0.3 μm (Ziegler et al. 2010). Thus, the implantation of projectile ions into the ice could be ensured.

Three samples, S^{7+}-over-irradiated residue, S^{7+}-irradiated ice and Ar^{7+}-irradiated ice were produced. It should be noted that the warming process could impact the incorporation of the Sulphur but in the same way in ices and residues. However, the difference in organic fingerprints for the S^{7+}-over-irradiated residue, S^{7+}-irradiated ice and Ar^{7+}-irradiated ice samples strongly indicates that different chemical processes occur dependent of the ion type. The samples were produced as following:

For S^{7+}-over-irradiated residue:

1. Deposition of H_2O:CH_3OH:NH_3 = 2:1:1 at 10 K
2. Irradiation with Ar^{7+} ions for 30 minutes at 10 K
3. Warming up to 300 K (warm-up rate = 0.5 K/minute) → formed organic residue results
4. Cooling down to 10 K (again)
5. Irradiation of the residue with S^{7+} ions for 40 minutes
6. Warming up to 300 K (again, warm-up rate = 0.5 K/minute) → modified organic residue results (named "S^{7+}-over-irradiated residue")

For Ar^{7+}-irradiated ice (reference sample):

1. Deposition of H_2O:CH_3OH:NH_3 = 2:1:1 at 10 K
2. Irradiation with Ar^{7+} ions for 30 minutes at 10 K
3. Warming up to 300 K (warm-up rate = 0.5 K/minute) → formed organic residue results (named "Ar^{7+}-irradiated ice", reference sample)

For S^{7+}-irradiated ice:

1. Deposition of H_2O:CH_3OH:NH_3 = 2:1:1 at 10 K
2. Irradiation with S^{7+} ions for 30 minutes at 10 K
3. Warming up to 300 K (warm-up rate = 0.5 K/minute) → formed organic residue results (named "S^{7+}-irradiated ice")

The IGLIAS setup enabled in situ chemical analysis of the sample by a Bruker V70 Fourier Transform Infrared Spectrometer (IR spectroscopy). The evolution during the irradiation is monitored and validated by IR spectroscopy on both methanol and ammonia infrared absorption bands. Final residues, resulting from irradiated ices and over-irradiated organic residues, were kept under argon atmosphere in a stainless steel vessel to minimize oxidation prior to ESI-FT-ICR-MS analysis (de Marcellus et al. 2015).

Appendix A.2: ESI-FT-ICR-MS analysis

ESI-FT-ICR-MS (Electrospray ionization Fourier transform ion cyclotron resonance mass spectrometry) was used for in-depth molecular characterization of the organic matter formed within the residue, resulted from irradiated ices. High resolution mass spectrometry has been widely used for in-depth molecular characterization of extraterrestrial organic matter (Schmitt-Kopplin et al. 2010; Danger et al. 2013, 2016; Ruf et al. 2017; Fresneau et al. 2017; Ruf et al. 2018, 2019c; Gautier et al. 2020; Danger et al. 2020). FT-ICR-MS represents the highest performance in mass resolving power and mass precision among all mass spectrometers (Ruf et al. 2018). Negative ionization mode was used because CHNOS anions could have been detected with greater sensitivity compared to their cationic counterparts.

Organic residues were diluted in 50 μL methanol (extraction solvent, LC-MS grade; Fluka). This step was repeated four times. Most of the S^{7+}-over-irradiated residue got dissolved while the residue resulting from Ar^{7+}-irradiation got completely dissolved in methanol. The non-dissolved part of the S^{7+}-over-irradiated residue got then dissolved in 50 μL toluene, and subsequently diluted in methanol for analysis, as described below). Afterwards, an aliquot of 20 μL of the dissolved residue was diluted in 200 μL methanol. The solution was then taken by a micro-syringe and transferred by flow injection into the ESI source. A solvent methanol blank was measured in accordance to be able to detect the indigenous soluble organic matter in each residue sample.

Analyses were performed on a high-field FT-ICR-MS from Bruker Daltonics with a 12 Tesla magnet from Magnex. A time domain transient with four MWords was obtained and Fourier-transformed into a frequency domain spectrum. The frequency domain was then converted to a mass spectrum by the solariX control program of Bruker Daltonics. Ion excitation was generated in broadband mode (frequency sweep radial ion excitation) and 3000 scans were accumulated for each mass spectrum in a mass range of 147 to 1000 amu (atomic mass unit). Ions were accumulated for 300 ms before ICR ion detection. The pressure in the quadrupole/hexapole and ICR vacuum chamber was 3 x 10^{-6} mbar and 6 x 10^{-10} mbar, respectively.

The Electrospray ionization source was Apollo II from Bruker Daltonics. The methanol solutions were injected directly into the ionization source by means of a microliter pump at a flow rate of 120 μL h-1. A source heating temperature of 200 °C

was maintained and no nozzle-skimmer fragmentation was performed in the ionization source. The instrument was previously externally calibrated by using arginine negative cluster ions (5 mg L^{-1} arginine in methanol).

Mass spectra with m/z from 147 to 1000 amu were calibrated externally and internally to preclude alignment errors. Subsequently, mass spectra were exported to peak lists at a signal-to-noise ratio 3 (S/N = 3). Mass resolving power was 400,000 at m/z = 400 with a mass accuracy of <200 ppb, enabling the separate detection of isobars differing by less than the mass of an electron (Ruf et al. 2017). Practically, this approach enables a direct assignment of molecular compositions with C, H, N, O, and S atoms (and isotopologues in natural abundance) for each individual exact mass (m/z value).

Molecular formulas were assigned from exact m/z values for each peak in batch mode by an in-house software tool (Tziotis et al. 2011) and validated via the senior-rule approach/cyclomatic number (Senior 1951). For formula assignment, 42% of all formulas have an error of ±0.1 ppm, 69% an error of ±0.2 ppm, and 98% an error of ±0.5 ppm, with all assigned formulas having an error of ±1 ppm (Figure B.1).

Data mining on organosulfur (CHNOS) compounds represent those m/z signals which were uniquely detected in the S^{7+}-over-irradiated residue and absent in the Ar^{7+}-irradiated ice (reference sample), as performed using LibreOffice or Python (Van Rossum & Drake Jr 1995). The double bond equivalent (DBE) was calculated according DBE = C - (H/2) + (N/2) + 1. Further details on the assignment of molecular formulas from FT-ICR-MS big data and their visualization in astrochemical context are given in previous studies (Ruf et al. 2018).

Appendix A.3: Molecular network analysis

Theoretical ion masses of the above assigned molecular formulas were used for molecular network reconstruction (transformation analysis using mass difference calcuations). Theoretical ion masses (nodes) were connected by edges (transformations) if their mass differences were equal (±0 ppm) to the theoretical mass differences of ΔCH_2, ΔH_2, ΔO, ΔH_2O, ΔNH, ΔCO_2, ΔS (ΔCH_2 = 14.015650 amu, atomic mass unit, ΔH_2 = 2.01565 amu, ΔO = 15.994915 amu, ΔH_2O = 18.010565 amu, ΔNH = 15.010899 amu, ΔCO_2 = 43.98983 amu, ΔS = 31.972071 amu) representing chemical transformations. Then, ΔCH_2, ΔH_2, ΔO, ΔH_2O, ΔNH, ΔCO_2 represent potential reactions building up homologous series of a chemical family, while ΔS represents a possible reaction when a sulfur ion is implanted during the irradiation process. Transformations probing was performed via an in-house code using Python (Van Rossum & Drake Jr 1995). Molecular networks were laid out using the Cytoscape software, version 3.8.2 on Ubuntu (Prefuse Force Directed Layout) (Shannon et al. 2003).

Appendix B: Supporting figures

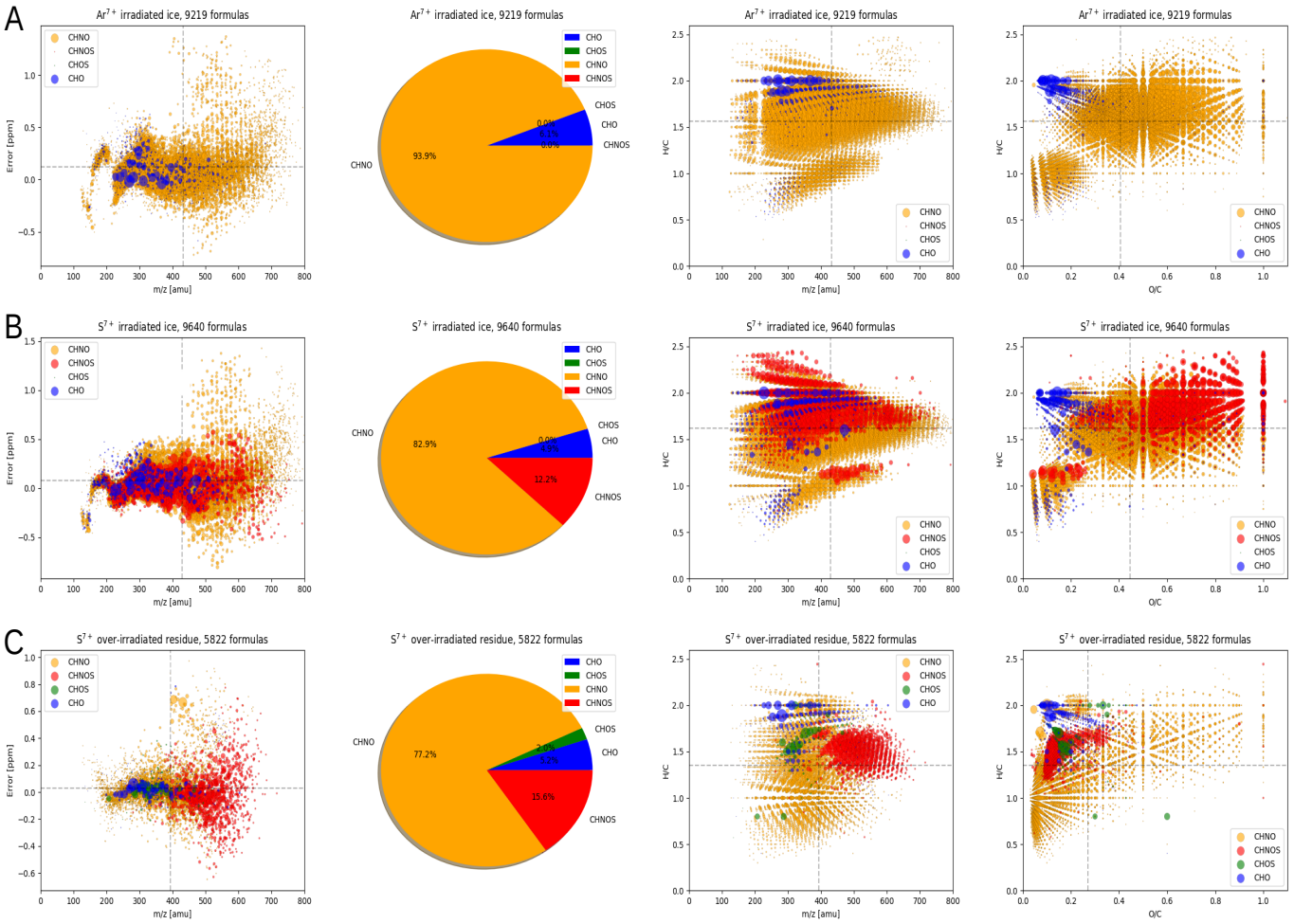

Fig. B.1. Overview of chemical families present in the S^{7+}-over-irradiated residue: (A) Ar^{7+}-irradiated ice); (B) S^{7+}-over-irradiated residue); (C) S^{7+}-irradiated ice). Error vs. m/z plots are shown for validation the molecular formula annotation. Pie charts represent the distributing of different chemical families, and H/C vs m/z and H/C vs O/C illustrate the distribution of the chemical families CHO, CHNO, CHOS and CHNOS. Dashed lines represent mean values.

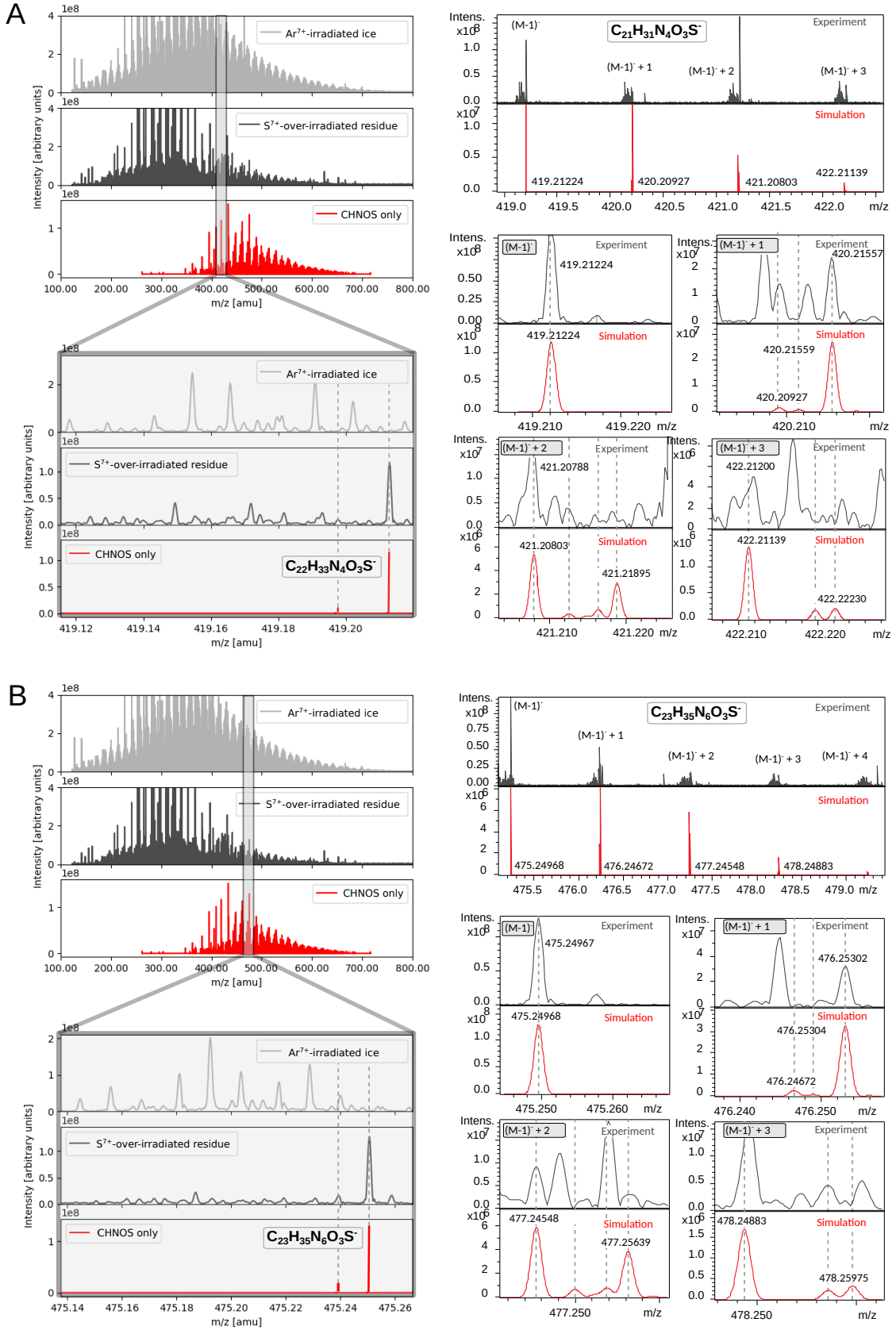

Fig. B.2. Detection of $[C_{21}H_{31}N_4O_3S]^-$ (A) and $[C_{23}H_{35}N_6O_3S]^-$ (B) molecule ions. Detection by ESI-FT-ICR-MS of organosulfur (CHNOS) compounds, exemplarily shown for $[C_{21}H_{31}N_4O_3S]^-$ (B) and $[C_{23}H_{35}N_6O_3S]^-$ (B) molecular ions. The CHNOS-only spectrum (left panel, 3rd row, red) illustrates 908 CHNOS-assigned m/z signals that were absent in the Ar^{7+}-irradiated ice (reference sample). For the isotopic fine structure: darkgray = experimental spectrum; red = simulated isotopic pattern.

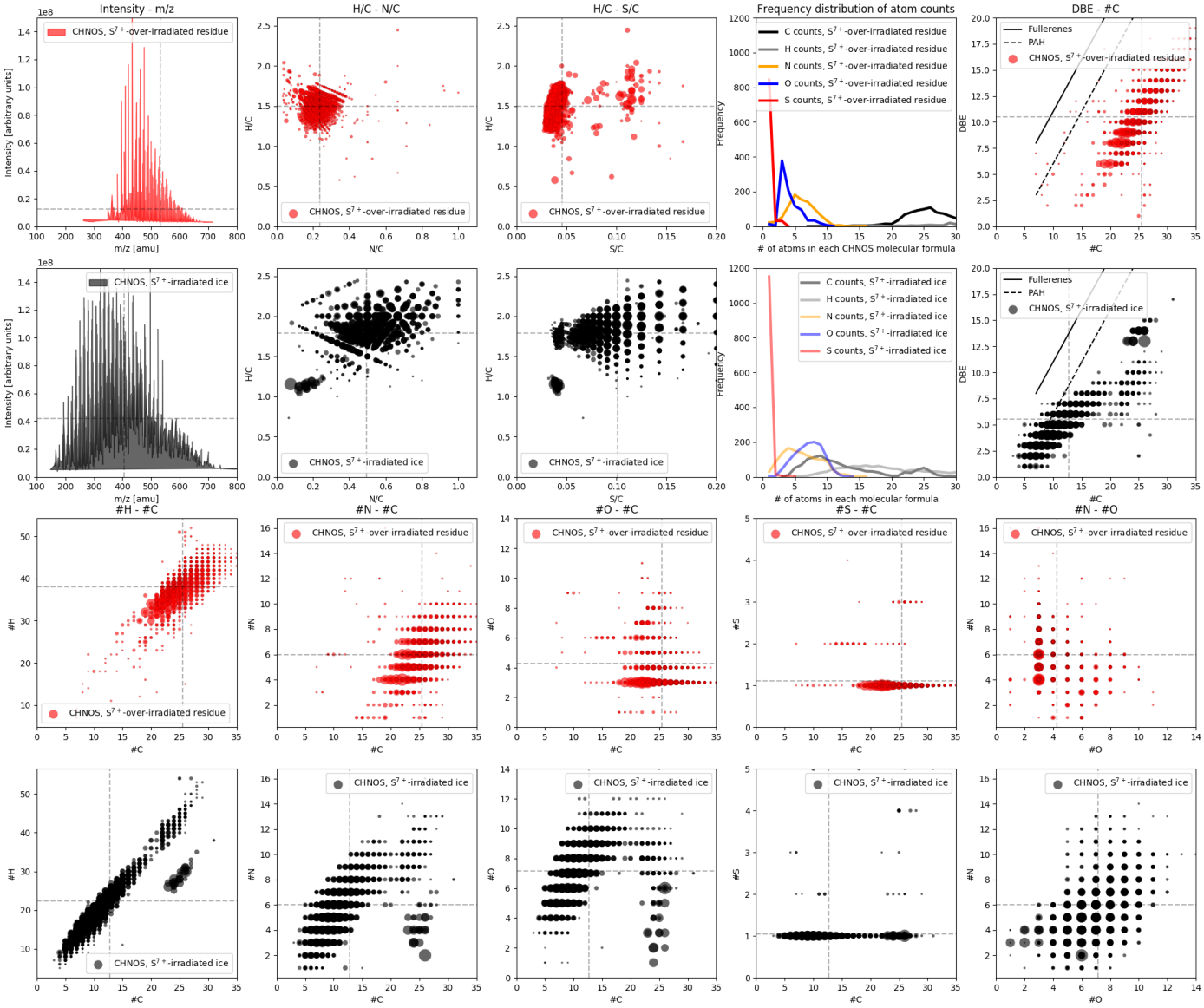

Fig. B.3. Characteristics of CHNOS compounds formed on residues (red, 1st and 3r row) or inside ices (black, 2nd and 4th row) - detailed plots. 1st-2nd row, from left to right: Intensity-m/z, H/C-N/C, H/C-S/C plots, frequency distribution of atom counts, DBE-#C plot. 3rd/4th row; from left to right: #H-#C, #N-#C, #O-#C, #S-#C and #N-#O plots. Dashed lines represent mean values.

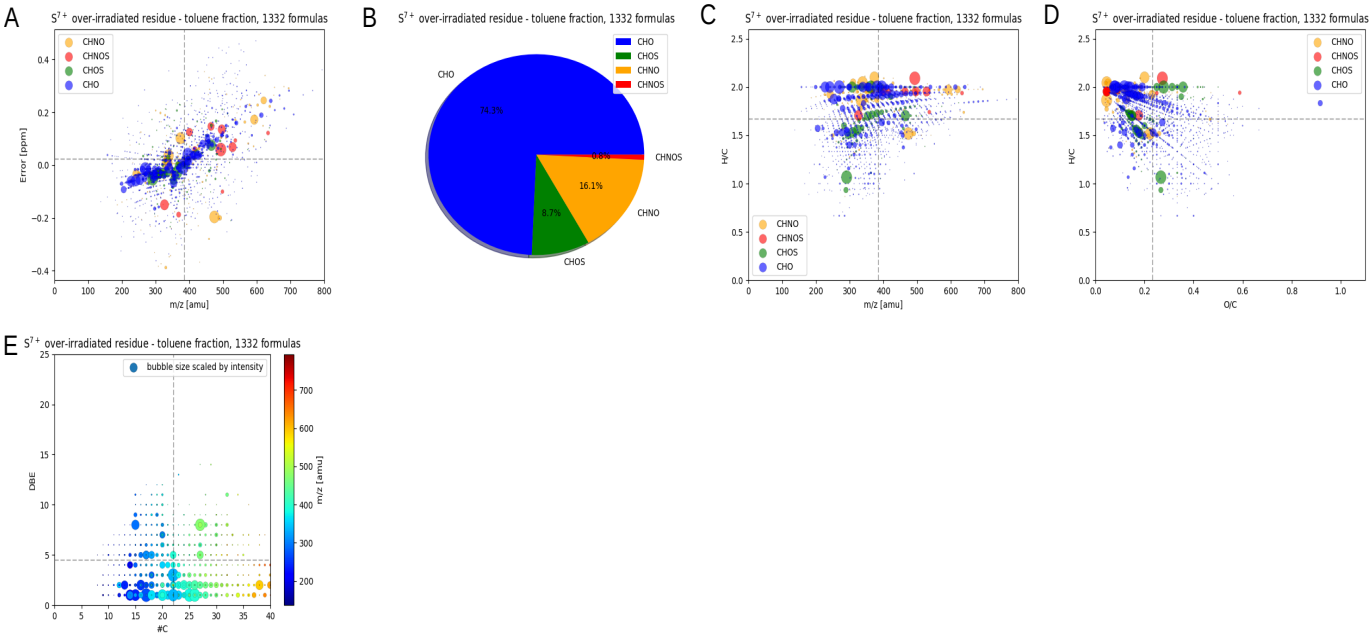

Fig. B.4. Overview of chemical families present in the toluene fraction of the S^{7+}-over-irradiated residue. (A) Error vs m/z plot for validating the molecular formula annotation. (B) Pie chart representing the distributing of different chemical families. H/C vs m/z (C) and H/C vs O/C (D) representation of the chemical families CHO, CHNO, CHOS, and CHNOS. Dashed lines represent mean values.

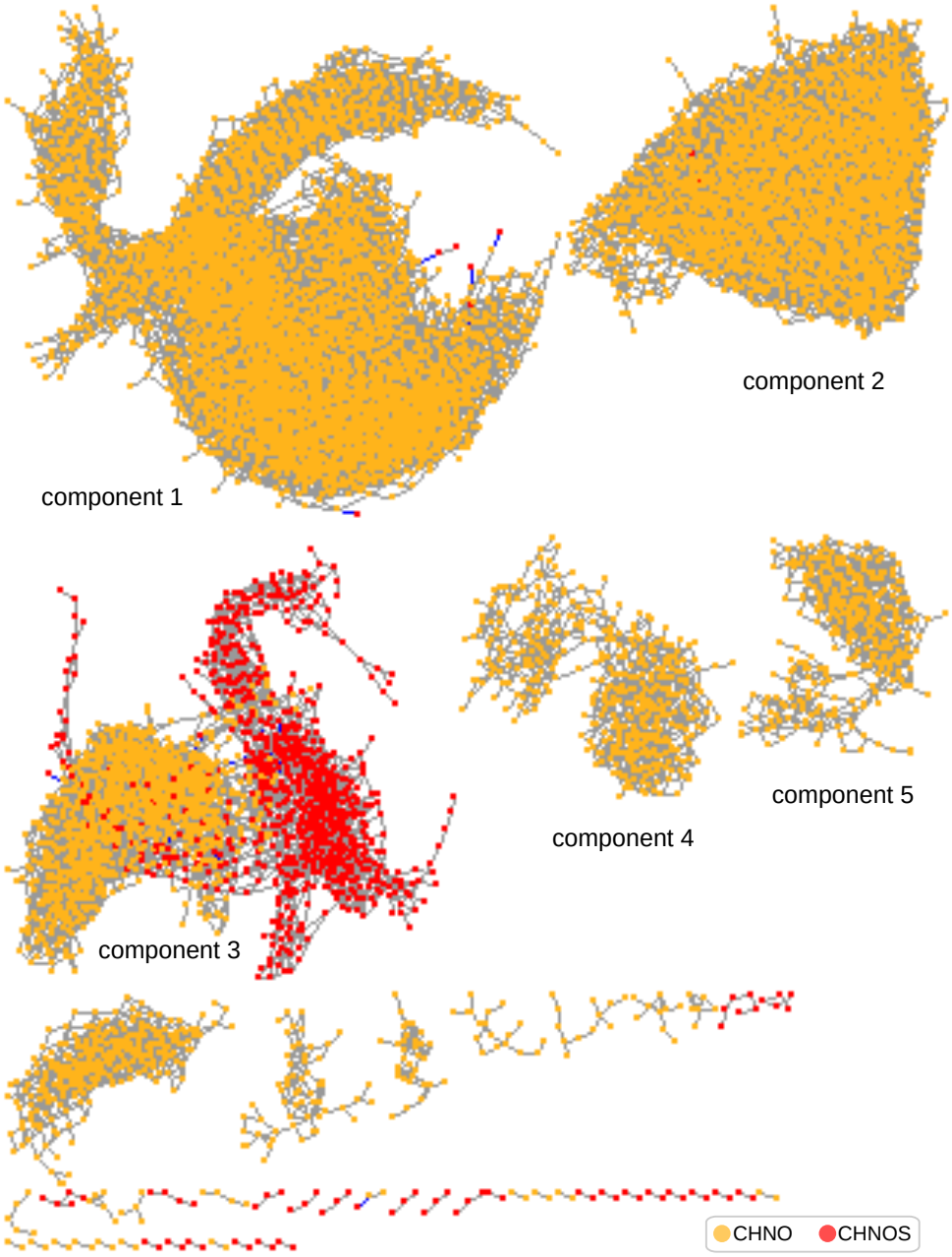

Fig. B.5. Complete molecular network, departed into 53 different components. Component number is sorted by size of the subnetwork.

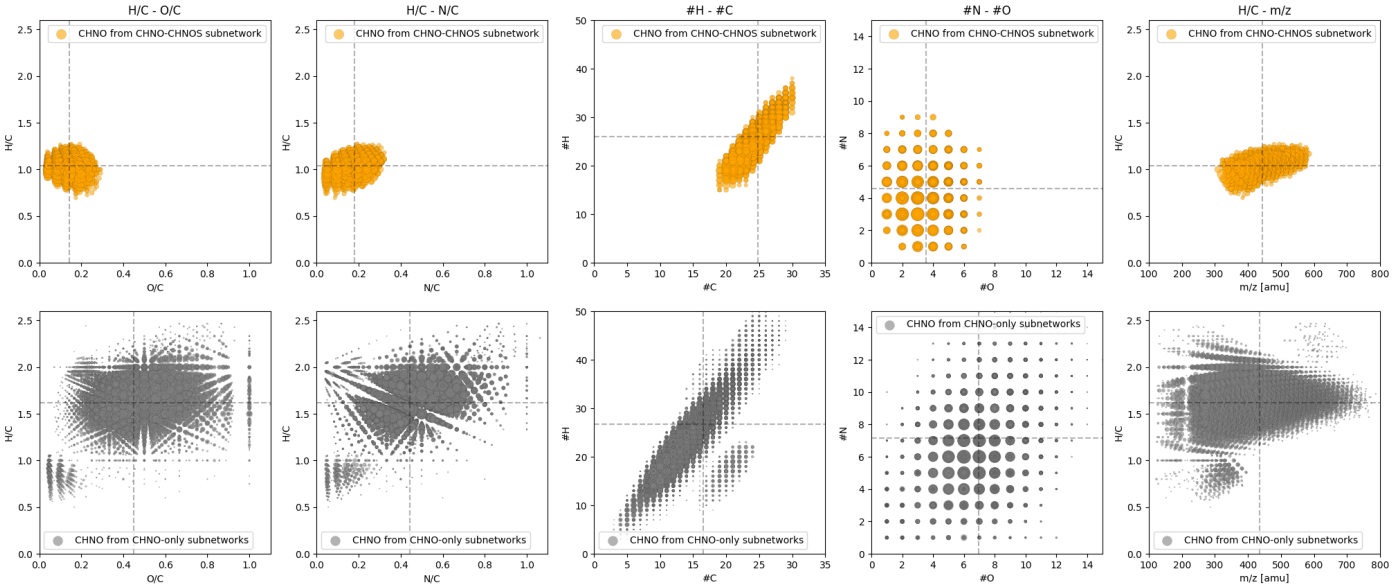

Fig. B.6. CHNO compound characteristics differentiating CHNOS precursors (1st row, orange) and non-CHNOS precursors (2nd row, gray). From left to right: H/C-O/C, H/C-N/C, #H-#C, #N-#O, H/C-m/z plots. Two groups of CHNO compounds (CHNOS precursors (direct and indirect ones), orange, and non-CHNOS precursors, gray) have been identified via molecular network analysis (see details in main text "CHNO-CHNOS molecular network" and Methods section "Molecular network analysis"). Dashed lines represent mean values.

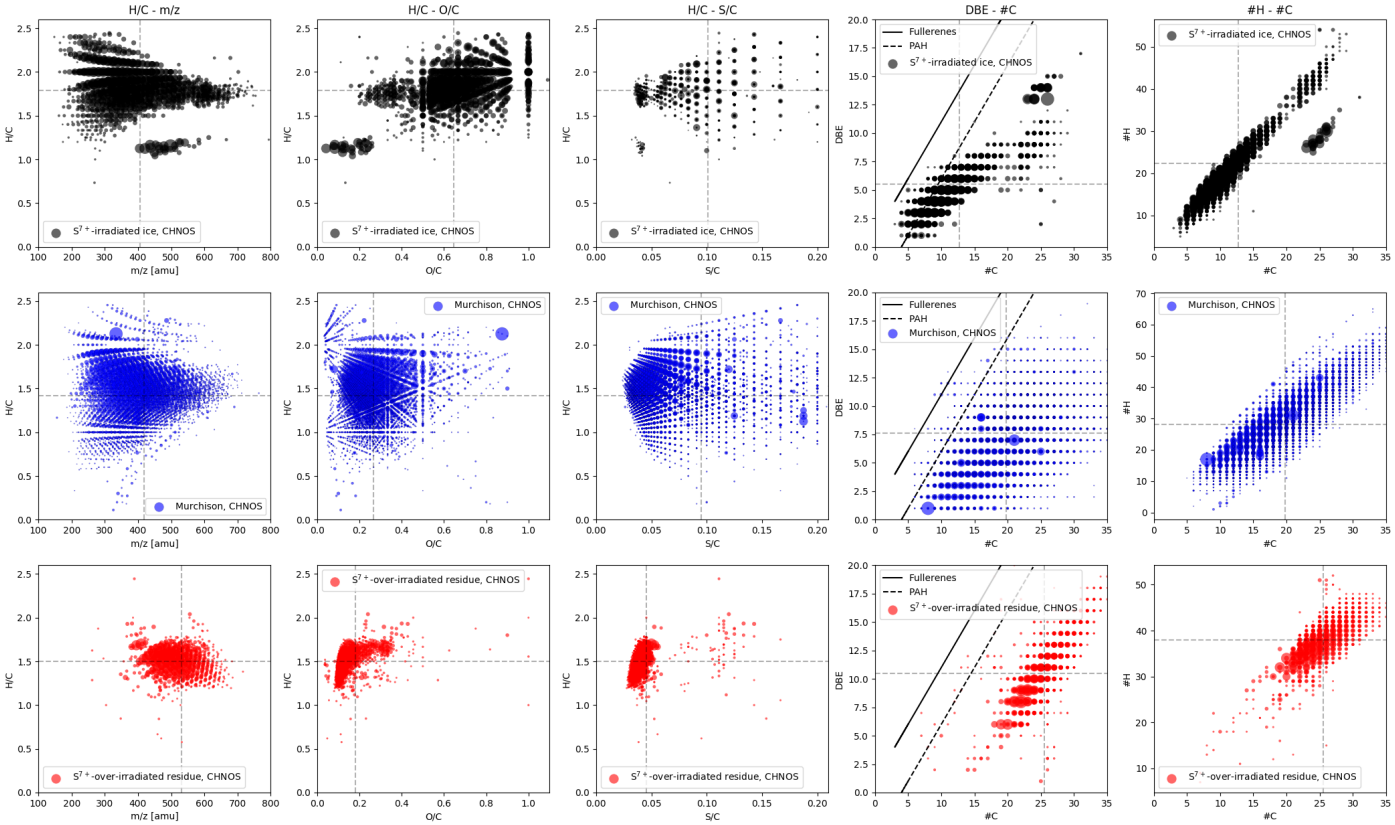

Fig. B.7. Relationship between organosulfur compounds (CHNOS) from S^{7+}-irradiated ices, Murchison meteorite and S^{7+}-over-irradiated residues - detailed plots. Dashed lines represent mean values.